The Synthesis, Mesomorphism, and Characterization by X-ray Diffraction and Freeze-Fracture Electron Microscopy of Polycatenar Liquid Crystals of Silver(I) Showing Columnar and Cubic Mesophases

Bertrand Donnio,[†] Benoit Heinrich,[‡] Thaddée Gulik-Krzywicki,*[,§] Hervé Delacroix,*[,§] Daniel Guillon,*[,‡] and Duncan W. Bruce*[,†]

Department of Chemistry, University of Exeter, Stocker Road, Exeter EX4 4QD, UK; IPCMS, Groupe des Materiaux Organiques, 23 rue du Loess, BP 20CR, 67037 Strasbourg Cedex, France; and Centre de Génétique Moléculaire, CNRS, 91198 Gif-sur-Yvette Cedex, France

Received May 8, 1997. Revised Manuscript Received August 4, 1997[⊗]

Complexation of 3,4-dialkoxystilbazoles to Ag^{I} has led to a new series of polycatenar, metal-containing liquid crystals. The complexes were found to show mainly cubic and columnar mesophases, although short-chain homologues showed a different behavior due to a dissociation of one ligand in the melt. On cooling from the mesophase, some of the complexes formed a glassy state, rather than crystallizing. The mesophases were characterized by a combination of optical microscopy, differential scanning calorimetry, X-ray diffraction and freeze-fracture electron microscopy. Freeze-fracture electron microscopy was successful in identifying the symmetry of the cubic phase as $Ia\bar{3}d$, while the transition between the cubic and columnar phase was studied by a combination of X-ray diffraction and dilatometry, allowing the proposal of a model for the transition between these two phases using their observed epitaxial relationship and requiring undulation of the columnar phase as proposed previously for lyotropic mesophases.

Introduction

Metal-containing liquid crystals,[1] studied extensively since the mid-1980s, represent a new and very important development in the study of liquid-crystalline materials. Properties such as enhanced electronic polarizability[2] and hyperpolarizability,[3] dichroism,[4] paramagnetism,[5] and reactivity have been observed or are expected to result on inclusion of a metal center in a liquid-crystal compound.

As part of our work in this area,[6] we have carried out extensive studies[7] of the mesomorphic complexes formed by reaction of 4-alkoxystilbazoles with various salts of silver(I) (Figure 1). These complexes have been shown to exhibit a remarkably diverse mesomorphism for mesogens that are formally ionic, and nematic, S_A, S_C, G, and cubic phases have been observed, of which the nematic and cubic are particularly noteworthy. Thus,

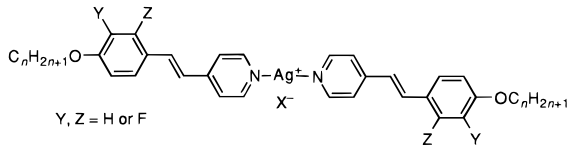

Figure 1. Structure of alkoxystilbazole complexes of silver(I).

these complexes are virtually unique examples[7b,8] of ionic compounds showing a nematic phase, while cubic phases are rather rare in thermotropic liquid crystals. In this paper, we report an extension of these studies with the synthesis and mesomorphism of a new series of complexes based on 3,4-dialkoxystilbazoles and having the typical structure of polycatenar mesogens. Furthermore, we present the results of physical studies used to investigate the mesophases. In particular we

[†] University of Exeter.
[‡] Groupe des Materiaux Organiques.
[§] Centre de Génétique Moléculaire.
[⊗] Abstract published in *Advance ACS Abstracts,* October 15, 1997.

(1) Bruce, D. W. *Inorganic Materials*, 2nd ed.; Bruce, D. W., O'Hare, D., Eds.; Wiley; Serrano, J.-L. Ed; *Metallomesogens*; VCH: Weinheim, 1996.
(2) Bertram, C.; Bruce, D. W.; Dunmur, D. A.; Hunt, S. E.; Maitlis, P. M.; McCann, M. *J. Chem. Soc., Chem. Commun.* **1991**, 69.
(3) Bruce, D. W.; Thornton, A. *Mol. Cryst. Liq. Cryst.* **1993**, *231*, 253.
(4) Bruce, D. W.; Dunmur, D. A.; Hunt, S. E.; Maitlis, P. M.; Orr, R. *J. Mater. Chem.* **1991**, *1*, 857.
(5) Ovchinnikov, I. V.; Galyametdinov, Y. G.; Ivanova, G. I.; Yagfarova, L. M. *Dokl. Akad. Nauk. SSSR* **1984**, *276*, 126. Galyametdinov, Y. G.; Ovchinnikov, I. V.; Bolotin, B. M.; Etingen, N. B.; Ivanova, G. I.; Yagarova, L. M. *Izv. Akad. Nauk. SSSR, Ser. Khim.* **1984**, 2379. Ovchinnikov, I. V.; Galyametdinov, Y. G.; Bikchantaev, I. G. *Izv. Akad. Nauk. SSSR Ser. Fiz.* **1989**, *53*, 1870. Galimov, R. M.; Bikchantaev, I. G.; Ovchinnikov, I. V. *Zh. Strukt. Khim.* **1989**, *30*, 65.
(6) See e.g.: Morrone, S.; Guillon, D.; Bruce, D. W. *Inorg. Chem.* **1996**, *35*, 7041. Bruce, D. W.; Holbrey, J. D.; Tiddy, G. J. T. *J. Chem. Soc., Dalton Trans.* **1995**, 1769. Bruce, D. W.; Wali, M. A.; Wang, Q. M. *Chem. Commun.* **1996**, 2505. Bruce, D. W.; Liu, X. H. *J. Chem. Soc., Chem. Commun.* **1994**, 729. Rowe, K. E.; Bruce, D. W. *J. Chem. Soc., Dalton Trans.* **1996**, 3913.
(7) (a) Bruce, D. W.; Dunmur, D. A.; Lalinde, E.; Maitlis, P. M.; Styring, P. *Nature (London)* **1986**, *323*, 791. (b) Bruce, D. W.; Dunmur, D. A.; Maitlis, P. M.; Styring, P.; Esteruelas, M. A.; Oro, L. A.; Ros, M. B.; Serrano, J. L.; Sola, E. *Chem. Mater.* **1989**, *1*, 479; **1991**, 3, 378. (c) Bruce, D. W.; Dunmur, D. A.; Hudson, S. A.; Lalinde, E.; Maitlis, P. M.; McDonald, M. P.; Orr, R.; Styring, P. *Mol. Cryst. Liq. Cryst.* **1991**, *206*, 79. (d) Bruce, D. W.; Dunmur, D. A.; Hudson, S. A.; Maitlis, P. M.; Styring, P. *Adv. Mater. Opt. Electron* **1992**, *1*, 37. (e) Adams, H.; Bailey, N. A.; Bruce, D. W.; Davis, S. C.; Dunmur, D. A.; Hempstead, P. D.; Hudson, S. A; Thorpe, S. *J. Mater. Chem.* **1992**, *2*, 395. (f) Bruce, D. W.; Hudson, S. A. *J. Mater. Chem.* **1994**, *4*, 479. (g) Bruce, D. W.; Donnio, B.; Hudson, S. A.; Levelut, A. M.; Megtert, S.; Petermann, D.; Vèber, M. *J. Phys. II (France)* **1995**, *5*, 289. (h) Bruce, D. W.; Donnio, B.; Guillon, D.; Heinrich, B.; Ibn-Elhaj, M. *Liq. Cryst.* **1995**, *19*, 537.
(8) To our knowledge, one other example is known: Ghedini, M.; Pucci, D. *J. Organomet. Chem.* **1990**, *395*, 105.

S0897-4756(97)00300-1 CCC: $14.00 Published 1997 by the American Chemical Society

wished to derive an understanding of the molecular organization within the cubic and columnar mesophases in order to try to understand the driving forces leading to these transitions.

It has long been known that the symmetries of the thermotropic mesophases are dependent on the shape of the mesogens. Indeed, ellipsoidal molecules give rise to nematic and lamellar structures[9] (N, S_A, S_B, S_C, ...) while discoid molecules are more likely to display columnar mesomorphism[10] where different symmetries are obtained as a result of the columnar organization (e.g., hexagonal, rectangular). However, none of these two structural types of molecules shows mixed mesomorphism, namely lamellar and columnar mesophases, within an homologous series. This remained true until the discovery of the so-called phasmids by Malthête[11] and biforked mesogens by Nguyen.[12] These molecules, later collectively named *polycatenar mesogens*,[13] can be seen as compounds having a molecular structure intermediate between a rod and a disk. This type of liquid crystal represents a "missing link" between the classical ellipsoid and discoid mesogens, as evidence by their remarkable liquid-crystalline properties. Indeed, their mesomorphism includes nematic (N), smectic C (S_C), cubic (Cub), and columnar (Col) mesophases between room temperature to ca. 200 °C.

In particular, tetracatenar[14] systems (four chains) represent an excellent example of the competition between calamitic and columnar phases. Thus, for the most part, short-chain-length homologues display N and S_C phases while longer homologues exhibit only columnar phases. At intermediate chain lengths, this competition is clearly observed by the appearance of a frustrated mesophase, namely, the cubic phase. Tetracatenar molecules can be regarded as being amphiphilic[15] in character in the sense that segregation of the aromatic and aliphatic parts tends to occur in the mesophase. This results in the curvature of the paraffinic−aromatic interface (recall the curvature of a circle is the inverse of its radius: a straight line is a circle with infinite radius and with zero curvature, while a small circle has a small radius and a large curvature). By increasing *n*, the number of carbon atoms in the aliphatic chains, the curvature of the paraffinic−aromatic interface increases, resulting in the destabilization of the calamitic phase in favor of the columnar phase via, in some cases, the cubic phase, as found in surfactant systems. This resemblance to lyotropic mesomorphism is intuitive as in both cases molecular associations govern the polymorphism and similarity in the phases sequences have been observed (two-dimensional oblique or rectangular lattices and three-dimensional cubic phases are inserted between the lamellar and the hexagonal phases).

Cubic phases are quite common in amphiphilic systems and have been extensively studied,[16] being located in different parts of the binary phase diagram according to their mean interfacial curvature.[17] One can distinguish two types of cubic phases: the micellar (I_1) cubic phase, located between the micellar solution (L_1 phase) and the hexagonal (H_1) phase, and the bicontinuous (V_1) cubic phase, between the lamellar (L_α) phase and the hexagonal (H_1) phase. They also can be inverse or normal depending on the polarity of the solvent used and on the shape of the amphiphile. Both types of cubic phase appear transparent and optically isotropic under a polarizing microscope, often making their identification troublesome, although the phases are very viscous and can therefore be distinguished from the isotropic solution. The only unequivocal means of characterization of these phases are small- and wide-angle X-ray diffraction (SAXS and WAXS) and freeze-fracture electron microscopy (FFEM). As a result of such studies, new models based on periodic minimal surfaces have been proposed and fully accepted in order to understand these three-dimensional structures and the transitions with adjacent phases (lamellar, hexagonal).[18]

However, thermotropic cubic phases are not so well understood due mainly to their rare appearance. There are now about a dozen compounds displaying this mesophase that have been so far reported in literature. The most famous ones are some derivatives of the 4-alkoxy-3-nitrobiphenyl-4′-carboxylic acids and 4-alkoxy-3-cyanobiphenyl-4′-carboxylic acids,[19] but this phase occurs with three derivatives of the 1,2-bis[(4-alkoxy)-benzoyl]hydrazine,[20] the hexa-*O*-pentanoylscylloinositol,[21] a few derivatives of the ellagic acids,[22] and some tetracatenar compounds.[14] Very recently, new compounds have been reported to display this phase such as some silver complexes described above,[7c,f] *cis*,*cis*-(3,5-dihydroxycyclohexyl)-3,4-dialkoxybenzoates (two chains diol),[23] one member of the series of 4,4′-bis(*ω*-hydroxyalkoxy)azoxybenzene[24] derivatives, many homologues of the big family of the glycolipids,[25] and finally some bis-

(9) Gray, G. W.; Goodby, J. W. *Smectic Liquid Crystals: Textures and Structures*; Leonard Hill Publishers: Glasgow, 1984. Zorkii, P. M.; Timofeeva, T. V.; Polishchuk, A. P. *Russ. Chem. Rev.* **1989**, *58*, 1971.

(10) Destrade, C.; Gasparoux, H.; Foucher, P.; Nguyen, H. T.; Malthête, J. *J. Chim. Phys.* **1983**, *80*, 137. Levelut, A. M. *J. Chim. Phys.* **1983**, *80*, 149. Destrade, C.; Foucher, P.; Gasparoux, H.; Nguyen, H. T.; Levelut, A. M.; Malthête, J. *Mol. Cryst. Liq. Cryst.* **1984**, *106*, 121. Chandrasekhar, S. *Liq. Cryst.* **1993**, *14*, 3.

(11) Malthête, J.; Levelut, A. M.; Nguyen, H. T. *J. Phys. Lett. (France)* **1985**, *46*, 875.

(12) Nguyen, H. T.; Destrade, C.; Levelut, A. M.; Malthête, J. *J. Phys. (France)* **1986**, *47*, 553.

(13) (a) Gasparoux, H.; Hardouin, F.; Destrade, C.; Nguyen, H. T. *New J. Chem.* **1992**, *16*, 295. (b) Malthête, J.; Nguyen, H. T.; Destrade, C. *Liq. Cryst.* **1993**, *13*, 171.

(14) Levelut, A. M.; Fang, Y. *Colloid Phys.* **1990**, *7*, 225. Fang, Y.; Levelut, A. M.; Destrade, C. *Liq. Cryst.* **1990**, *7*, 265. Nguyen, H. T.; Destrade, C.; Malthête, J. *Liq. Cryst.* **1990**, *8*, 797.

(15) Hendrikx, Y.; Levelut, A. M. *Mol. Cryst. Liq. Cryst.* **1988**, *165*, 233. Skoulios, A.; Guillon, D. *Mol. Cryst. Liq. Cryst.* **1988**, *165*, 317.

(16) Fontell, K. *Colloid Polym. Sci.* **1990**, *268*, 264.

(17) Seddon, J. M.; Templer, R. H. *Philos. Trans. R. Soc. London A* **1993**, *344*, 377.

(18) Clerc, M.; Levelut, A.-M.; Sadoc, J. F. *J. Phys II (France)* **1991**, *1*, 1263.

(19) Gray, G. W.; Jones, B.; Marson, F. *J. Chem. Soc.* **1957**, 393. Diele, S.; Brand, P.; Sackmann, H. *Mol. Cryst. Liq. Cryst.* **1972**, *17*, 163. Etherington, G.; Leadbetter, A. J.; Wang, X. J.; Gray, G. W.; Tajbakhsh, A. *Liq. Cryst.* **1986**, *1*, 209. Kutsumizu, S.; Yamada, M.; Yano, S. *Liq. Cryst.* **1994**, *3*, 155.

(20) Demus, D.; Gloza, A.; Hartung, H.; Hauser, A.; Rapthel, I.; Wiegeleben, A. *Cryst. Res. Technol.* **1982**, *16*, 1445. Demus, D.; Diele, S.; Grande, S.; Sackmann, H. *Adv. Liq. Cryst.* **1983**, *6*, 1.

(21) Kohne, B.; Praefcke, K.; Billard, J. *Z. Naturforsch.* **1986**, *41b*, 1036.

(22) Billard, J.; Zimmermann, H.; Poupko, R.; Luz, Z. *J. Phys. (France)* **1989**, *50*, 539. Zimmermann, H.; Billard, J.; Gutman, H.; Watchtel, E. J.; Poupko, R.; Luz, Z. *Liq. Cryst.* **1992**, *12*, 245.

(23) Lattermann, G.; Staufer, G. *Mol. Cryst. Liq. Cryst.* **1990**, *191*, 199. Schellhorn, M.; Lattermann, G. *Liq. Cryst.* **1994**, *17*, 529. Staufer, G.; Schellhorn, M.; Lattermann, G. *Liq. Cryst.* **1995**, *18*, 519.

(24) Yano, S.; Mori, Y.; Kutsumizu, S. *Liq. Cryst.* **1991**, *9*, 907.

(25) Fischer, S.; Fischer, H.; Diele, S.; Pelzl, G.; Jankowski, K.; Schmidt, R. R.; Vill, V. *Liq. Cryst.* **1994**, *17*, 855.

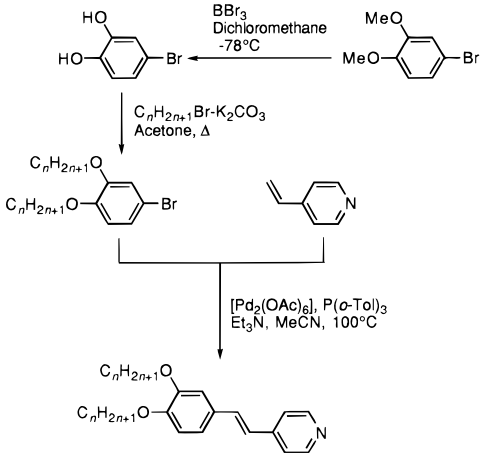

Figure 2. Preparation of 3′,4′-dialkoxy-4-stilbazole via the Heck reaction.

(swallow-tailed) liquid crystals.[26] One can notice that most of these compounds possess a rather conventional structure, making the prediction of the occurrence of the cubic phase almost impossible. However, we can remark that in general they all possess a greater paraffinic/aromatic ratio than the classical ellipsoid molecules, which can be a major driving force in the creation of curvatures at the interface leading to two- and three-dimensional structures. We must also consider the influence of H-bonding associations, the ionic character, and the strong amphiphilicity present in these systems, on the formation of the cubic phase.

In common with their lyotropic counterparts, thermotropic cubic phases show a very well-developed, long-range, three-dimensional order, although X-ray shows a diffuse reflection at ca. 4.5 Å, corresponding to the liquid-like state of the hydrocarbon chains. They can be considered equivalent to the inverse bicontinuous lyotropic cubic phases, and thus similar models may be used for their description, for example, interlocked 3-D rod networks[27] and infinite periodic minimum surfaces, IPMS[28]). There have so far been three different cubic space groups which have been identified in thermotropic liquid crystals ($Ia\bar{3}d$, $Im\bar{3}m$ and $Pm\bar{3}$ (or $Pm\bar{3}m$)). In a recent part of our studies on silver-containing liquid crystals, we described an X-ray determination of a cubic monodomain shown by some derivatives,[7g] which were easily indexed in the $Ia\bar{3}d$ cubic space group (Q^{230}), similar to some lyotropic and thermotropic materials.

Following studies on polycatenar materials, it was realized that by increasing the number of chains grafted on the same rodlike core, the formation of cubic and columnar mesophases could be promoted. We therefore undertook the synthesis of a series of polycatenar silver complexes based on 3,4-dialkoxystilbazoles, the synthesis and proposed structure of which are shown in Figures 2 and 3. Preliminary results of these studies have already appeared.[7h]

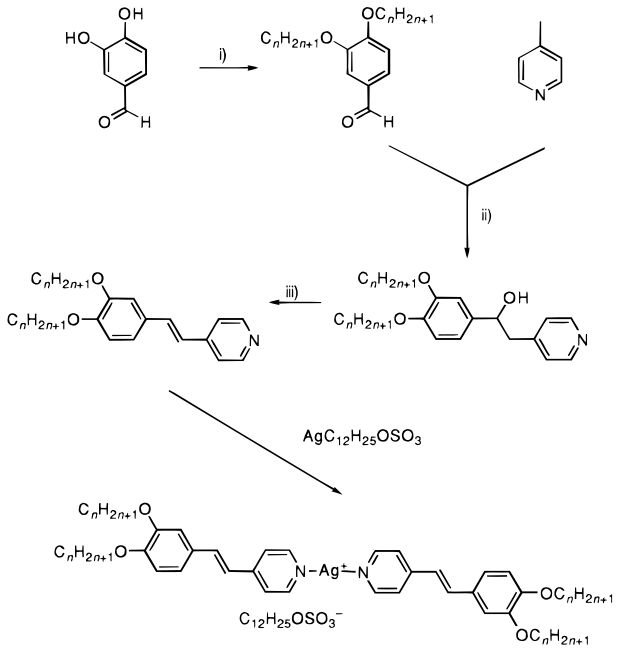

Figure 3. Preferred synthesis of the dialkoxystilbazoles and their silver complexes. i: $C_nH_{2n+1}Br/K_2CO_3$/2-pentanone/Δ. ii: LDA/−78 °C/THF; H_2O/HCl/RT. iii: PPTS/toluene/Δ.

Synthesis

The ligands and complexes were mainly prepared according to Figure 3. Thus, in the preferred procedure, 3,4-dihydroxybenzaldehyde was reacted with the appropriate 1-bromoalkane under Williamson ether conditions to give the related 3,4-dialkoxybenzaldehyde. This was subsequently reacted at low temperature with the anion of 4-methylpyridine to give, after workup, the alcohol. Dehydration with pyridinium *p*-toluenesulfonate then afforded the product, 3′,4′-dialkoxy-4-stilbazole, as an exclusively trans product (^{1}H NMR $J_{AB} = 16.5$ Hz). Initially, the dialkoxystilbazoles had been prepared (Figure 2) via a palladium-catalyzed Heck coupling between 3,4-dialkoxybromobenzene and 4-vinylpyridine, with the dialkoxybromobenzene being obtained in two steps from 3,4-dimethoxybromobenzene (bromoveratrole), namely, demethylation with BBr_3 followed by alkylation under Williamson ether conditions. This latter route was eventually abandoned due to the shorter reaction times, higher yields, and easier purification associated with the former method.

The complex was then obtained by reaction of 2 equiv of the ligand with silver dodecyl sulfate (from silver nitrate and sodium dodecyl sulfate) in dichloromethane at room temperature.

Mesomorphism

Unlike the 4′-alkoxy-4-stilbazoles[29] which showed a limited mesomorphism, none of the 3′,4′-dialkoxy-4-stilbazoles, [St(*n*-3,4)], was mesomorphic. Curiously however, many of the longer-chain dialkoxystilbazoles showed similar clearing temperatures to the "parent" (mono)alkoxystilbazoles, and also to 4′-alkoxy-3′-fluoro-4-stilbazoles, as shown in Table 1.

The complexation of these new 3,4-dialkoxystilbazoles to silver(I) dodecyl sulfate gave rise to a new series of

(26) Weissflog, W.; Pelzl, G.; Letko, I.; Diele, S. *Mol. Cryst. Liq. Cryst.* **1995**, *260*, 157.

(27) Luzzati, V.; Spegt, P. A. *Nature (London)* **1967**, *215*, 701. Tardieu, A.; Billard, J. *J. Phys. (France)* **1976**, *C3*, *37* 79. Lydon, J. E. *Mol. Cryst. Liq. Cryst. Lett.* **1981**, *72*, 79. Guillon, D.; Skoulios, A. *Europhys. Lett.* **1987**, *3*, 79.

(28) Sadoc, J. F.; Charvolin, J. *J. Phys. (France)* **1986**, *47*, 683. Charvolin, J.; Sadoc, J. F. *J. Phys. (France)* **1987**, *48*, 1559. Charvolin, J. *Contemp. Phys.* **1990**, *31*, 1. Charvolin, J. *Mol. Cryst. Liq. Cryst.* **1991**, *198*, 145.

(29) Bruce, D. W.; Dunmur, D. A.; Lalinde, E.; Maitlis, P. M.; Styring, P. *Liq. Cryst.* **1988**, *3*, 385.

Table 1. Clearing Temperatures (°C) of Different Series of Stilbazoles

	n											
	1	2	3	4	5	6	7	8	9	10	11	12
St(*n*-4)	136	153	112	95	85	73	86	75	86	84	86	85
St(*n*-3,4)	132	128	115	105	79	78	79	82	83	83	85	87
St(3F-*n*-4)	84	97	85	63	69	56	78	64	85	70	86	69

Table 2. Thermal Data for [Ag(St(*n*-3,4))$_2$][dos]

n	transition	*T*/°C	ΔH/kJ mol^{-1}	ΔS/J mol^{-1} K^{-1}
1[a]	Crys − Crys + I	108		
	Crys + I − I	123		
	(I−N)	(95)		
2[a]	Crys − Crys + I	103		
	Crys + I − I	107		
	(I−N)	(98)		
3	Crys − I	108	36.6	96.2
4	Crys − Cub	90	27.9	76.7
	Cub − I	102	2.1	5.6
5	Crys − Cub	76	26.6	76.2
	Cub − I	116	3.3	8.4
6	Crys − Cub	61	29.3	87.6
	Cub − ϕ_h	118	2.6	6.6
	ϕ_h − I	153	1.0	2.3
7	Crys − Cub	66	30.5	89.8
	Cub − ϕ_h	127	3.1	7.8
	ϕ_h − I	158	1.8	4.1
8	Crys − Crys′	56	1.2	3.6
	Crys′ − Cub	70	27.7	80.7
	Cub − ϕ_h	115	2.9	7.5
	ϕ_h − I	164	1.4	3.1
9	Crys − Crys′	58	7.6	23.0
	Crys′ − Cub	75	31.9	91.6
	Cub − ϕ_h	107	2.4	6.4
	ϕ_h − I	169	2.2	5.1
10	Crys − Crys′	64	33.7	99.9
	Crys′ − Cub	81	36.9	104.4
	Cub − ϕ_h	97	2.2	5.9
	ϕ_h − I	169	2.5	5.8
11	Crys − Crys′	69	25.6	74.8
	Crys′ − ϕ_h	82	38.4	108.2
	ϕ_h − I	176	2.6	5.9
12	Crys − Crys′	71	54.8	159.4
	Crys′ − ϕ_h	83	10.6	29.7
	ϕ_h − I	172	3.7	8.4

[a] The molar enthalpies and entropies of transition have not been calculated due to the different species giving rise to the mesomorphism.

silver-based metal-containing liquid crystals. The first point to be noted is that the complexation of the nonmesomorphic ligand to silver(I) dodecyl sulfate gives a very strongly mesomorphic material, once more illustrating an important aspect of the introduction of metals into liquid crystals, namely, the induction of mesomorphism. The thermal behavior of these complexes is collected in Table 2, and the phase diagram is shown in Figure 4.

In general, the thermal stability of the complexes was good, and under the conditions we employed, there was no evidence of decomposition for any of the samples on cooling from either the mesophase or the isotropic liquid. As a precaution, the complexes were stored in the dark, although stability to light did not appear to be a problem.

In principle, these complexes can be identified as tetracatenar **2(*mp*) + 2(*mp*)** systems (i.e., two chains at each end of the molecule in the meta and para positions) according to the nomenclature proposed for polycatenar systems by Malthête et al.,[13b] but this classification is confused by the presence of the dodecyl sulfate anion, which we assume acts as a lateral group

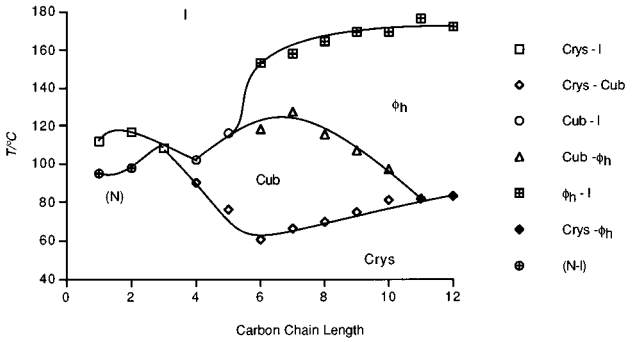

Figure 4. Phase diagram for [AgSt(*n*-3,4)$_2$][DOS]. For $n = 1$ and 2, the melting points shown correspond to the temperature at which the 2:1 complex falls apart (see text).

and for which there is no direct analogy in conventional polycatenar systems. Thus, similar to organic tetracatenar **2(*mp*) + 2(*mp*)** materials, the mesomorphism is strongly dependent on the chain length. The optical microscopy of [Ag{St(*n*-3,4)}$_2$][DOS] suggested the following mesomorphic behavior.

The propyloxy homologue did not show any liquid-crystalline properties and cleared straight to the isotropic liquid at 108 °C, while the butoxy and pentoxy homologues ($n = 4$ and 5) displayed only a cubic mesophase, assigned on the basis of its apparent optical isotropy. Further, it was observed to grow in as square-edged monodomains in the crystalline phase and with a large hysteresis; equally, we observed distorted air bubbles resulting from the high viscosity of the phase (a consequence of the cubic symmetry of the mesophase). The thermal stability of the phase increased considerably from $n = 4$ ($\Delta T = 12$ °C) to $n = 5$ ($\Delta T = 40$ °C). Finally, on cooling, the phase grew in from the isotropic liquid with 20 °C of supercooling and persisted to room temperature where crystallization occurred; these transitions were reproducible.

For the hexoxy−decyloxy homologues ($n = 6-10$), the crystals melted into the cubic phase and then underwent another transition to give a columnar phase, postulated on the basis of its optical texture. Thus, on heating, a broken focal-conic texture was observed, while on slow cooling from the isotropic liquid, large monodomains with a well-defined, pseudo-focal-conic texture joined together four-by-four through their apexes was seen. In addition, some areas presented a mosaic texture, characteristic of this type of structure. On further cooling, the cubic phase grew in very slowly with some supercooling. For the undecyloxy−dodecyloxy homologues ($n = 11-12$), only a columnar phase was observed with the same optical texture as described above. The thermal stability of the columnar phase increased with chain length.

Homologues having a chain length of $n = 8$ to $n = 12$ all showed a crystal−crystal transition as observed by DSC. However the crystal phase adjacent to the cubic or columnar phases never appeared on subsequent heating and cooling cycles.

By contrast, for $n = 1$ and 2, the complexes showed a completely different behavior. These complexes were synthesized in the same way as all the others and gave an elemental analysis that corresponded to a 2:1 complex. This structure was also confirmed by the relative intensities of the protons around 4 ppm, which arise from the Ph−O−CH_2− protons of the stilbazole and the

O_3SO-CH_2- protons of the dodecyl sulfate chain. Integrations of 6:1 (stilbazole:anion) for the methoxy and 4:1 (stilbazole:anion) for the ethoxy derivatives were found. However, on heating, a first melting event was observed giving a two-phase, isotropic-plus-solid-state, system. At a higher temperature, a second melting event occurred at a temperature that corresponded to the melting point of the free stilbazole, to give a fully isotropic state. On cooling, however, a nematic phase was observed over a few degrees, below the first melting event. From this behavior, we therefore concluded that the 2:1 complex was formed during the synthesis and that this was thermally unstable with respect to dissociation into monoligand complex plus free ligand. This is supported by the NMR data, which showed only one set of ligand protons. Thus, the first melting is postulated to correspond to the thermal dissociation leaving the monoligand complex, which melts. At the second melting point, the free ligand also melts to give a fully isotropic state. On cooling and at a temperature below the first melting point, a homogeneous nematic phase is observed, which suggests that the 2:1 complex reforms and gives rise to the nematic phase. Crystallization is then the crystallization of the 2:1 complex.

Attempts to prepare the 1:1 complex directly by stirring 1 equiv of the ligand with 1 equiv of the silver dodecyl sulfate yielded a 1:1 complex as evidenced by NMR which showed the relative intensities in the 4 ppm region to be 2:1 for the ethoxy complex. The complex was found to melt directly to the isotropic liquid at 118 °C. No evidence of similar behavior with higher homologues was ever observed.

Thus, the phase diagram could be divided into five different domains:

$n = 1, 2$, monotropic nematic phase

$n = 3$, no mesomorphism

$n = 4$ and 5, one cubic phase only

$6 \leq n \leq 10$, a cubic and a columnar phase

$n \geq 11$, only the columnar phase

In common with other **2(*mp*)** + **2(*mp*)** polycatenar systems, the bis(3′,4′-dialkoxy-4-stilbazole)silver(I) dodecyl sulfate ([Ag(St(*n*-3,4))$_2$][DOS]) mesogens showed cubic and columnar phases, but by contrast, no S_C phases were seen. We attributed the last observation to the presence of the lateral chain (dodecyl sulfate anion) in combination with the chain in the 3-positions which would tend to act to reduce the lateral associations necessary for smectic phase formation. A useful comparison is then made with the mesomorphism of the analogous complexes of the 4-alkoxystilbazoles, where for $n \geq 4$, a S_C phase was seen. Thus, the lateral alkyl sulfate chain alone is insufficient to suppress smectic phase formation, and thus, the 3-alkoxy chains clearly play a pivotal role in the determining the thermal stability of the S_C phase in these systems.

A common observation with all of these complexes was their relatively low melting point (61−90 °C) by comparison with the related, "parent", bis(4′-alkoxy-4-stilbazole)silver(I) dodecyl sulfate,[7c] which melt at around 110−140 °C. This shows that the two chains in the 3-position strongly perturb the stability of the crystal phase in the complex although not, as noted above, in the free ligand. Another important difference with the previously studied series[7] is that this new series is the first to display mesomorphism with both 2- and 3-dimensional structures. Here, the broadening of the molecules has led to a different kind of molecular association, which is discussed below. The high values of the enthalpies and entropies of transitions were expected as first the mesophases possess either 2- or 3-dimensional structures involving strong first order transitions and second due to the massive molecular reorganization from one phase to another. Interestingly in this series, we did not observe the metastable S_4 phase. The S_4 phase is commonly observed in association with the cubic mesophase of thermotropic mesogens and, according to our recent studies,[30] appears to have tetragonal symmetry. As little is known about the S_4 phase, we cannot speculate on the reason for its nonappearance in these new complexes.

Another observation was that on cooling, homologues with $4 \leq n \leq 8$, glassy states were formed rather than crystalline states. These states were evidenced by the retention of the isotropic texture on cooling, which did not give way to a crystalline form. In fact, in some samples, the glassy state was found to persist for many months (>24 at the time of writing) without any evidence of crystallization.

DSC

Because of the hysteresis in transition temperatures of the cubic phase and, to a lesser extent, of the columnar phase, DSC analysis was performed at intermediate rates on both heating and cooling cycle, typically 3 or 5 K min^{-1}. The DSC curves for the complexes showing the glassy state exhibited, on cooling, a shift in the baseline corresponding to the glass transition, and we were just able to measure ΔCp. All the glasses were cubic and therefore isotropic. For $n = 4$ and 5, a cold crystallization peak was observed on the second heating, leading to the behavior described above. The glass transition temperature has been determined by DSC only for the hexoxy, heptoxy, and octyloxy homologues. These three compounds did not show a recrystallization peak, but the crystal-to-cubic phase transition on the second heat.

X-ray Studies

Following to the observations from polarizing microscopy, the hexagonal columnar structure was confirmed by X-ray diffraction: up to five reflections, corresponding to the squared spacing ratios 1, 3, 4, 7, 9, and to the indexation $(hk) = (10), (11), (20), (21), (30)$, were observed in the patterns. The structural parameters are collected in Table 3. Since each columnar core contains ionic species, rodlike ligands, and aliphatic parts, the stacking period should be larger than typically found[31] for columnar cores solely formed by hard, rodlike cores (about 4.7 Å, i.e., the thickness of a single layer).

(30) Donnio, B., Bruce, D. W., Levelut, A.-M., *Liq. Cryst.* **1997**, *22*, 753.

(31) (a) Cruz, C.; Figueirinhas, J. L.; Sebastião, P. J.; Ribeiro, A. C.; Noack, F.; Nguyen, H. T.; Heinrich, B.; Guillon, D. *Z. Naturforsch.* **1996**, *5A*, 155. (b) Heinrich, B.; Guillon, D.; Cruz, C.; Ribeiro, A. C.; Nguyen, H. T., to be published.

Table 3. Structural Data for the Hexagonal and Cubic Phases from X-ray Diffraction Experiments

n	*T*/°C	phase	lattice parameter/Å[a]
4	90	Cub	72.5
5	90	Cub	75.0
6	50	Cub	79.0
	60	Cub	78.6
	70	Cub	78.1
	80	Cub	77.8
	90	Cub	77.5
	100	Cub	77.0
	110	Cub	76.5
7	90	Cub	80.3
7	130	ϕ_h	35.7
8	90	Cub	83.1
8	130	ϕ_h	36.8
9	90	Cub	86.0
9	130	ϕ_h	37.8
10	90	ϕ_h	41.4
10	130	ϕ_h	39.0
11	90	ϕ_h	42.5
	100	ϕ_h	41.6
	110	ϕ_h	41.0
	120	ϕ_h	40.6
	130	ϕ_h	40.1
	140	ϕ_h	40.0
	150	ϕ_h	39.7
12	90	ϕ_h	43.5
12	130	ϕ_h	41.2

[a] Refers to the intercolumnar distance for the ϕ_h phase, and the lattice parameter for the cubic phase.

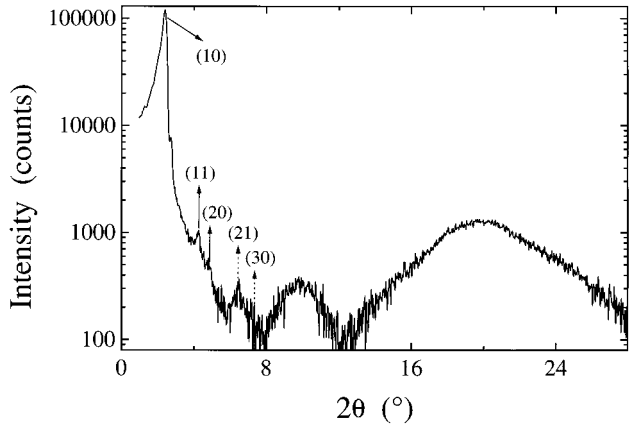

Figure 5. X-ray pattern in the hexagonal columnar phase, at 90 °C, for the chain length $n = 11$.

Thus, besides the diffuse reflection at about 4.5 Å occurring from the packing of the alkyl chains, a diffuse reflection at about 9.0 Å was observed at 90 °C for the homologue with undecyloxy chains (Figure 5). Because of the sensitivity of the sample to thermal degradation in the X-ray beam, it was not possible to determine the location of the diffuse reflection at higher temperatures and to follow the evolution of the stacking period with temperature.

From the isotropic texture and from the relatively high viscosity, the other phase was assumed to be a cubic mesophase. This assumption was also verified by X-ray diffraction whereby up to six reflections, corresponding to the squared spacing ratios 3, 4, 8, 10, 11, 13, could be observed in the patterns. Structural data are collected in Table 3. From freeze fracture experiments, the lattice was shown to be body-centered and the space group to be $Ia\bar{3}d$ (vide infra). Consistent with the extinction rules within this space group, the following indexation is proposed for the reflections in the X-ray diffraction patterns: $(hkl) = (211)$, (220), (400),

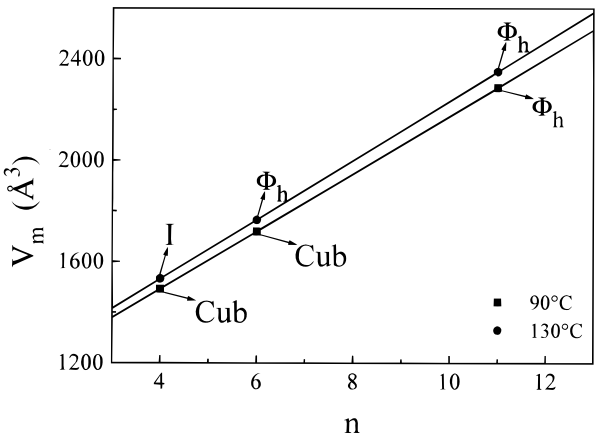

Figure 6. Molecular volume versus chain length at 90 °C and 130 °C (from dilatometry experiments).

(420), (332), (431). It should be pointed out that among the reflections allowed by this space group, the (321) and (422) reflections remained undetected. The fact that the (321) reflection is not observed is not entirely surprising as it often has a very low intensity as is also the case for the $Ia\bar{3}d$ cubic phase occurring frequently in lyotropic systems.[32] Nevertheless, the reflection (321) was the third most intense [after the reflections (211) and (200)] for other thermotropic systems showing an $Ia\bar{3}d$ cubic phase.[25] That the (422) reflection was not observed is a little more surprising, but as the structure factors for individual reflections will necessarily depend on the individual compound, then the fact that it is observed in other lyotropic systems does not necessarily mean that it should be expected every time an $Ia\bar{3}d$ space group is found.

Packing Study by Dilatometry

The variation with chain length and temperature of the spacings corresponding to the (100) reflections in the columnar phase and the (211) in the cubic phase and the variation of the molecular volume were followed in order to discuss the packing. The variation in the molecular volume is linear as a function of temperature for both phases (the columnar phase for the sample with undecyl substituents and the cubic phase for these with hexyl and butyl substituents) and as a function of chain length, despite the change from one mesophase to another (Figure 6). The slopes are in perfect agreement with the volume of the methylene groups in liquid alkanes (29.2 Å^3 at 130 °C, 28.4 Å^3 at 90 °C).[33] The variation of the spacings as a function of chain length can also be considered as linear (Figure 7); moreover, a continuity is observed between both spacing variations. Therefore, we can say that the local structural changes at the transition are rather minimal.

Hexagonal Columnar Phase

The first thing to note (Figure 8a) is that the columnar section, *s* (as defined in Figure 9 and also corresponding to the cross-sectional area of a column), decreases quite

(32) (a) Rançon, Y.; Charvolin, J. *J. Phys. (France)* **1987**, *48*, 1067. (b) Adam, M.; Delsanti, M.; Munch, J. P.; Durand, D. *J. Phys. (France)* **1987**, *48*, 1809. (c) Clerc, M.; Dubois-Violette, E. *J. Phys. II (France)* **1994**, *4*, 275.

(33) Doolittle, K. *J. Appl. Phys.* **1951**, *22*, 1471.

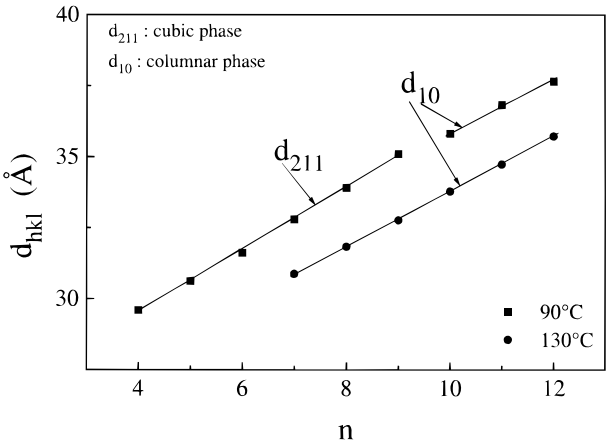

Figure 7. Spacings corresponding to the reflections (100) in the columnar phase and (211) in the cubic phase versus chain length at 90 °C and 130 °C.

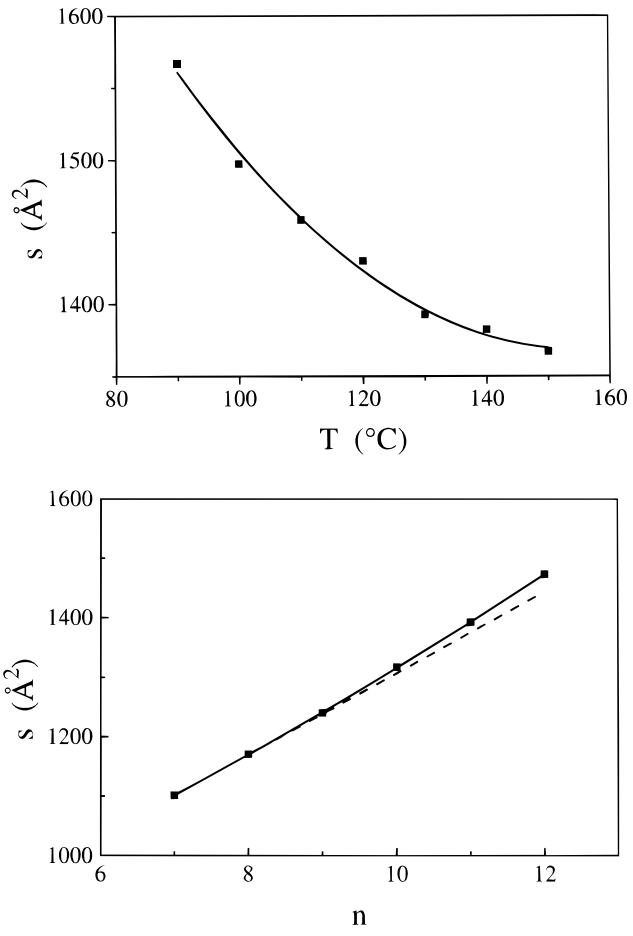

Figure 8. (a, top) Columnar section, *s*, versus temperature for the chain length $n = 11$. (b, bottom) Columnar section, *s*, versus chain length at 130 °C.

strongly with temperature. Therefore, if it is assumed that there are a constant number of molecules in the repeat unit, then as $N_H V_m = hs$ (where N_H is the number of molecules per repeat unit, V_m is the molar molecular volume, and h is the columnar repeat distance), then it can be deduced that h must also increase rather steeply. At $T = 130$ °C, h can therefore be evaluated as 10 Å, consistent with an increase from the value found by X-ray methods at 90 °C (9.0 Å). By using this value of h at 130 °C and the variations of V_m and s as a function of chain length at the same temperature, the number of molecules included in a repeat unit, N_H,

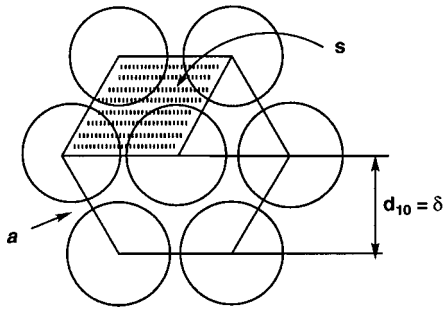

Figure 9. Schematic diagram to show the origin of the cross-sectional area, *s*.

is obtained either from extrapolation to zero chain length:

$$N_H = s^0 h [V^0]^{-1}$$

or from the slope of

$$N_H = \frac{ds}{dn} h \left(\frac{dV_m}{dn}\right)^{-1}$$

The latter calculation results in $N_H \sim 6.5$, while the former gives $N_H \sim 5.6$ or $N_H \sim 6.7$, depending upon whether the curvature in s has been neglected or approximated (by a parabolic fit of s), respectively. This would suggest that there are six molecules in the unit cell, each bearing four terminal chains and one dodecyl sulfate chain, giving a total of 30 chains.

A geometric relationship between the length of the hard cores, l, and N_H has previously been proposed and verified as follows.[34] By assuming that the rigid part of the column defines a circular cross-section of diameter l then its circumference must be πl. Further, each chain that radiates from, or crosses, that circumference (i.e., the core−chain interface) is assumed to require about 5.1 Å.[31,34] Thus, the number of chains which can be accommodated in the circular cross-section is $(\pi l)/5.1 = 15.4$ (for a rigid core evaluated, in this case, at 25 Å long). As we have five chains that can participate per complex (the chain connected to the anion being counted as a whole as it crosses the core−crown interface), then the model suggests $15.4/5 = 3.08 \approx 3$ complexes per repeat. However, the columnar spacing is evaluated as being 10 Å, suggesting that the repeat unit contains a double layer of complexes. Thus, the repeat unit is considered to contain 6 molecules, agreeing well with the experimental results presented above. The presence of the "double layer" also supports the idea that the silver complexes are present in the mesophase as dimers analogous to those found in the solid-state structure of monoalkoxystilbazoles complexed to silver octyl sulfate.[7e]

V_m can also be expressed as

$$V_m = V_0 + 6V_{DOS} + (24nV_{CH_2})$$

where V_0 is the volume of the rigid core, V_{DOS} is the volume of a dodecyloxy sulfate chain, n is the number of carbons atoms in the alkoxy chain, and V_{CH_2} is the volume of a CH_2 group. Therefore, plotting V_m against n gives a line of slope:

(34) Levelut, A.-M.; Malthête, J.; Destrade, C.; Nguyen, H. T. *Liq. Cryst.* **1987**, *2*, 877.

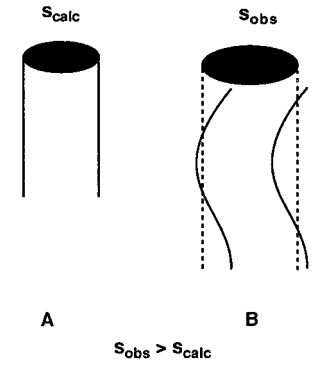

Figure 10. Schematic diagram to show the variation in *s* due to column undulation.

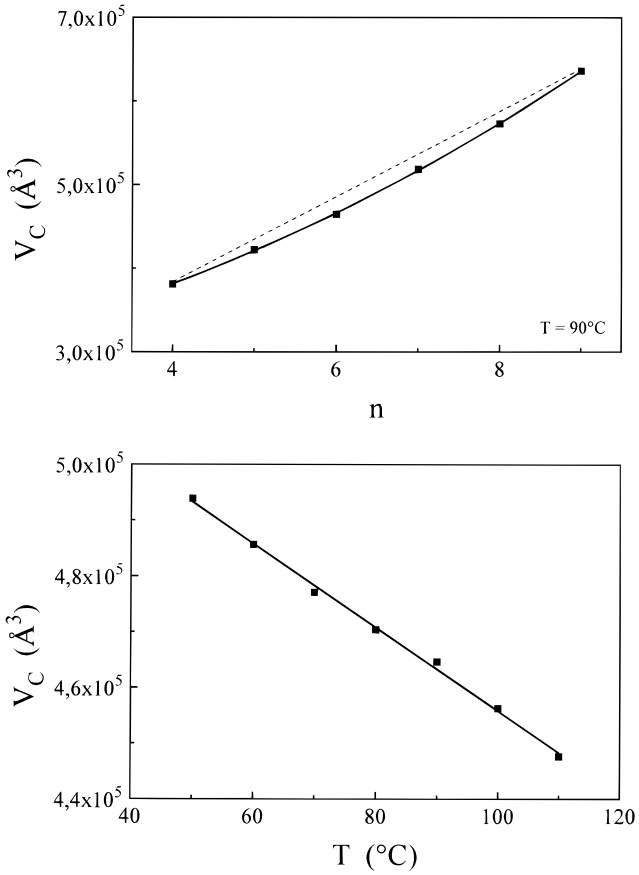

Figure 11. (a, top) $Ia\bar{3}d$ cubic lattice volume versus chain length at 90 °C. (b, bottom) $Ia\bar{3}d$ cubic lattice volume versus temperature for the chain length $n = 6$.

$$\text{slope} = 24V_{CH_2}/h$$

This allows the theoretical change in *s* with *n* to be evaluated. With $h = 10$ Å and $V_{CH_2} = 29.2$ Å, the calculated slope turns out to be 70 Å n^{-1}, giving a calculated value of $s = 1450$ Å^2 for $n = 12$. This line is plotted in Figure 8b and is consistent with the observed fact[35] that the columnar section, *s*, usually increases linearly as a function of chain length. However, in the present case (Figure 8b), the increase is steeper than expected and shows a slightly exponential form, showing that s is increasing more rapidly than expected and at a rate that increases with *n*. This therefore implied that

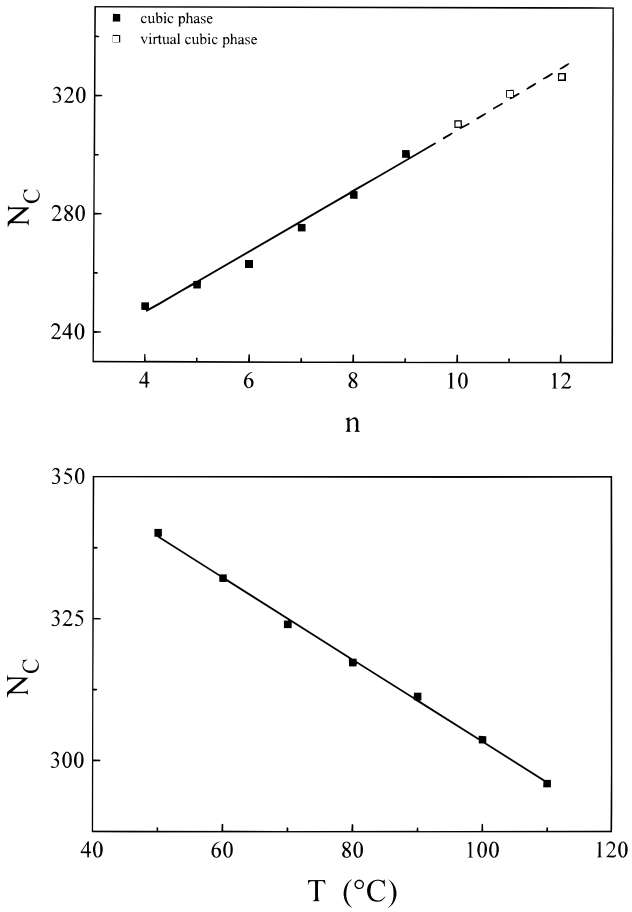

Figure 12. (a, top) Number of molecules included in the $Ia\bar{3}d$ cubic lattice (solid squares) and in the hexagonal columnar phase for a virtual $Ia\bar{3}d$ cubic lattice (open squares) versus chain length at 90 °C. (b, bottom) Number of molecules included in the $Ia\bar{3}d$ cubic lattice versus temperature for the chain length $n = 6$.

the stacking period, *h*, *decreases* as *n* increases (in one previously studied homologous series showing a linear increase in *s*,[35b] the invariance of *h* upon chain length was verified by dilatometry).

The unexpectedly rapid increase of *s* with *n* is explained by the proposal of the existence of an undulated structure for the columns as shown in the upper part of Figure 14. For a nonundulating column, *s* is simply the cross-sectional area of a column (Figure 10A), but for an undulating column, *s* is apparently greater as the column has a greater apparent width (Figure 10B). The origin of these undulations is that the surface area of a straight columnar core of these molecules would be larger than the inner area required by their attached chains, assuming the aliphatic tails to be confined in the {001} plane (plane normal to the columnar axis). This discrepancy can be compensated for by undulations of the columnar core, with the chains remaining in the {001} plane. As the effective volume occupied by the chains will increase with temperature, the mismatch will also reduce and so *s* will be expected to decrease, as observed (Figure 8a). Conversely, at lower temperatures, the amplitude of the undulations will increase.

An alternative explanation to compensate for the discrepancy in the areas would consist of the main stretching directions of the alkyl chains being both tilted out of the {001} plane. The stacking period would then

(35) (a) Weber, P.; Guillon, D.; Skoulios, A. *Liq. Cryst.* **1991**, *9*, 369. (b) Ibn Elhaj, M.; Guillon, D.; Skoulios, A.; Giroud-Godquin, A. M.; Maldivi, P. *Liq. Cryst.* **1992**, *11*, 731. (c) Heinrich, B.; Praefcke, K.; Guillon, D. *J. Mater. Chem.* **1997**, *7*, 1363.

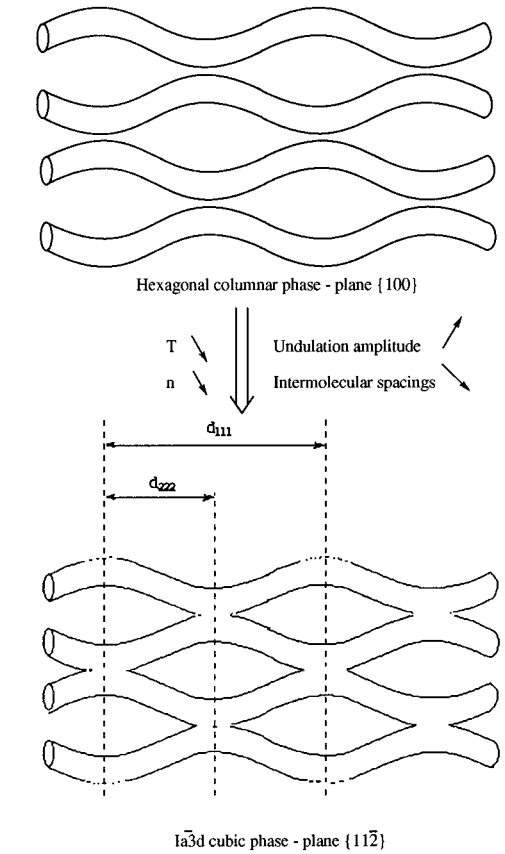

Figure 13. Undulating columnar cores model for the hexagonal columnar phase and model for the transition to the *Ia*$\bar{3}$*d* cubic phase.

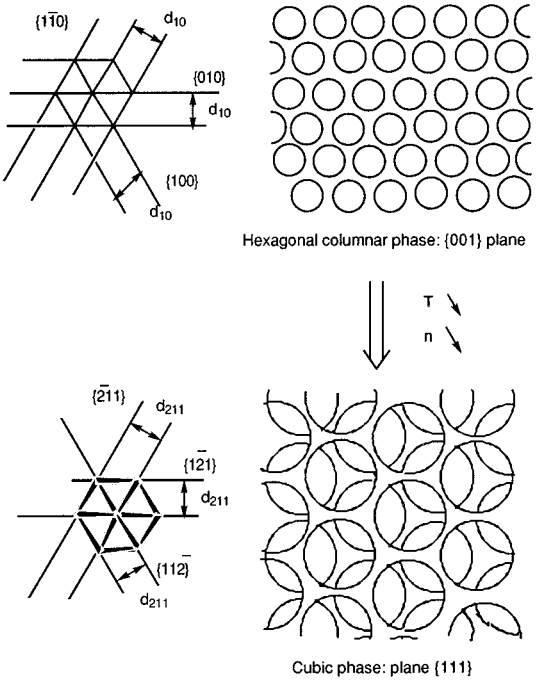

Figure 14. Relation between the hexagonal columnar and *Ia*$\bar{3}$*d* cubic phases.

be almost temperature-independent and the columnar area would therefore *increase* as predicted theoretically. The stacking within straight columnar cores would clearly be more stable than in undulating cores but would also be strongly destabilized by the amphipatic properties of rigid and aliphatic parts, as the model suggests greater interactions between the two different parts of the complex, which are, of course, unfavorable. These amphipatic properties would favor the rejection of the aliphatic tails along the hard core director, lying in the {001} plane in the case of a straight core, while tilted, out-of-plane main stretching directions of the alkyl chains would be imposed by the discrepancy in the areas. To support this idea, sublayer undulations instead of aliphatic tails tilting were also observed in the lamellar phase of water/surfactant systems.[36]

In the case of undulating columns, the local orientation of the rigid core is tilted out of the {001} plane, while the resultant orientation is in the {001} plane. The methylene groups next to the core remain aligned with the cores, but the methylene groups further from the hard cores become confined within the {001} plane. This confinement compensates the discrepancy in the areas by optimizing the microsegregation in space between aliphatic filling and columnar core, which are spread over the largest possible transverse area and stretched over the smallest possible height. Nevertheless, there are fluctuations and diffusion, and the microsegregation in space is not perfect but improves with increasing chain length, while the packing of the aliphatic tails becomes less influenced by the methylene groups next to the core. This would explain the increase in the undulation amplitude with increasing chain length, deduced from the curved dependence of s upon n.

Cubic Phase

The observation of a continuous variation between the spacings corresponding to the (211) reflections of the *Ia*$\bar{3}$*d* cubic phase and (100) of the hexagonal columnar phase is consistent with previous work on lyotropic systems on the epitaxial growth of one phase from the other,[37] the two planes having been found to transform into one another.

In addition, the continuous variation in both spacings implies that the cubic cell volume, V_C, is directly related to the area of the precursory columns s (see above) by the relationship

$$V_C = 3^{2.25} s^{1.5}$$

Consequently, the dependence upon chain length and temperature of V_C (Figure 11a,b) is similar to that of s, suggesting a similar interpretation.

The aliphatic filling becomes thicker with increasing chain length, leading to an increase in the distance between the knots in the {111} plane and in the cubic cell. Similar to the variation in s, a slight deviation from linear behavior is found for $V_C^{2/3}$ (Figure 12b), indicating that the area of the interface between the hard cores networks and the aliphatic filling decreases with increasing chain length, resulting in an additional increase of the distance between the knots in the {111} plane.

The area of the interface between the hard core networks and the aliphatic filling increases with increasing temperature. This results in a decrease in the distance between the knots in the {111} plane and in

(36) Kékicheff, P. *Mol. Cryst. Liq. Cryst.* **1991**, *198*, 131.
(37) Rançon, Y.; Charvolin, J. *J. Phys. Chem.* **1988**, *92*, 2646.

the cubic cell, which is partially compensated by the volume increase of the aliphatic filling.

The number of molecules included in the cubic cell, N_C, is directly obtained from the ratio of the cell volume, V_C, divided by the molecular volume, V_m, but can also be predicted from the continuity in the variation of the spacings d_{100} and d_{211}: the area of the {111} plan circumscribed in an elementary cubic unit corresponding to the transverse area of three columns in the {00*l*} plane of the columnar phase. Consequently, a volume equal to that of the cubic lattice contains as many repeat units (and therefore molecules in the columnar and in the cubic phases) as the ratio of the lattice area to the stacking period (the relation being deduced from that between V_C and *s*:

$$N_c = 3^{2.25} s^{1.5} V_m{}^{-1} = 3^{2.25} N_H s^{0.5} h^{-1}$$

The dependence of N_C upon chain length and temperature (Figure 12a,b) follows the influence of these parameters on *s* and *h* (on the thickness of the aliphatic filling on the area of the interface between the hard-core networks and the aliphatic filling) just discussed above. Moreover, the N_C values calculated from *s* and V_m in the columnar phase for a virtual cubic phase are in good agreement with the experimental values (Figure 11a), confirming the relation between the two types of structure.

Columnar-to-Cubic Phase Transition

A striking result of the packing study is that the variations in the packing parameters in the $Ia\bar{3}d$ cubic phase are just the continuation of those in the hexagonal columnar phase (see for instance Figure 12a and the immediately preceding paragraph). This suggests that large undulations of the columnar cores around the equilibrium axis preexist in the columnar phase, otherwise $s^{0.5}h^{-1}$ would increase drastically at the transition to the cubic phase and the theoretical N_C values in the columnar phase would be much smaller than the experimental values in the cubic phase instead of lying on the same line.

Whatever the origin of the undulations may be, the transition to the cubic phase obviously occurs when the amplitude of the undulations reaches the whole thickness of the aliphatic filling (Figure 13), which can happen either by decreasing the temperature or by shortening the chain length, i.e., mainly from increasing amplitude or from increasing thickness. At the closest approach of the columns, the chains, which are considered to be outside of the columns as drawn, can be accommodated by interdigitation between different columns, especially remembering that the undulation arises due to a mismatch between the surface area of the column defined by the core and that required by the chains.

The transition can then be considered by remembering the epitaxial relationship between the 10 and 211 spacings in the columnar and cubic phases, respectively, as indicated in Figure 14. As viewed in the upper part of the diagram showing the columnar phase, a coalescence can be considered between a central (shaded) column, and the three columns around it indicated by a cross, generating the 3-fold symmetry required of $Ia\bar{3}d$.[27,32a,37] Meanwhile, the three columns indicated by a small spot can also coalesce at a different height on the column to generate the other part of the 3-fold network of $Ia\bar{3}d$.

After the transition to the cubic phase, the area of the interface between the hard-core networks and the aliphatic filling decreases with decreasing temperature, just at the same rate as in the columnar phase. Nevertheless, while the decrease of the interface area should result from enhanced undulations in the columnar phase, it should occur from extended "junction areas" between the precursor columnar cores. Concerning the evolution by decreasing chain length, the extension of the "junction areas" seems obvious and the delaying of this extension by a poorer confinement of the aliphatic tails in the {111} plane may well explain the curvature in the variation of $V_C{}^{2/3}$ (vide supra). Further, it seems that the increase in *s* with increasing *n* and decreasing temperature is consistent with the form of the phase diagram in which the stability of the cubic phase falls off with increasing *n*, being overtaken by the crystal phase at $n > 10$.

Freeze-Fracture Electron Microscopy

Freeze-fracture electron microscopy has been used for many years to study liquid crystals, and the analysis of images of properly frozen samples displaying order in one or two dimensions were shown to be in excellent agreement with the structures determined by X-ray diffraction.[38] Nevertheless, a problem that remains is that the intrinsic resolution of the micrographs tends to be rather low, leading to problems of interpretation for complex, three-dimensional, liquid-crystalline structures such as cubic phases. However, the quality of the images can be considerably enhanced using image-filtering techniques based on correlation averaging, allowing a quantitative comparison of the electron microscopy structure to be made with that derived from X-ray diffraction experiments.[39] Moreover, information that is not available from the X-ray powder patterns, such as the presence of rotation axes and mirror planes in the unit cell, can be directly revealed, helping to narrow down the range of possible space groups. These methods, which are described in detail in ref 38c, have been applied successfully to both type I and type II bicontinuous[38] and micellar[40] cubic phases.

One of the main conclusions that can be drawn from that previous work is that different cubic phases display different, highly characteristic for a given space group, fracture behavior, namely, the frequency, appearances, and two-dimensional lattice type and dimensions of different fracture planes. This conclusion suggests that freeze-fracture electron microscopy, followed by appropriate image analysis, may be used for the determination of the type of lattices and the pres-

(38) Gulik-Krzywicki, T. *Biochim. Biophys. Acta* **1975**, *415*, 1. Gulik-Krzywicki, T.; Costello, J. *J. Microsc.* **1978**, *112*, 103. Gulik-Krzywicki, T.; Aggerbeck, L. P.; Larsson, K. *Surfactant in Solution*; Mittal, K., Lindman, B., Eds.; Plenum Press: New York, 1984; p 237.

(39) (a) Delacroix, H.; Gulik-Krzywicki, T.; Mariani, P.; Risler, J. L. *Liq. Cryst.* **1993**, *15*, 605. (b) Delacroix, H.; Gulik-Krzywicki, T.; Mariani, P.; Luzzati, V. *J. Mol. Biol.* **1993**, *229*, 526. (c) Gulik-Krzywicki, T.; Delacroix, H. *Biol. Cell.* **1994**, *80*, 193. (d) Delacroix, H.; Gulik-Krzywicki, T.; Seddon, J. M. *J. Mol. Biol.*, in press.

(40) Luzzati, V.; Vargas, R.; Gulik, A.; Mariani, P.; Seddon, J. M.; Rivas, E. *Biochemistry* **1992**, *31*, 279. Gulik, A.; Delacroix, H.; Kirschner, G.; Luzzati, V. *J. Phys. II (France)* **1995**, *5*, 445.

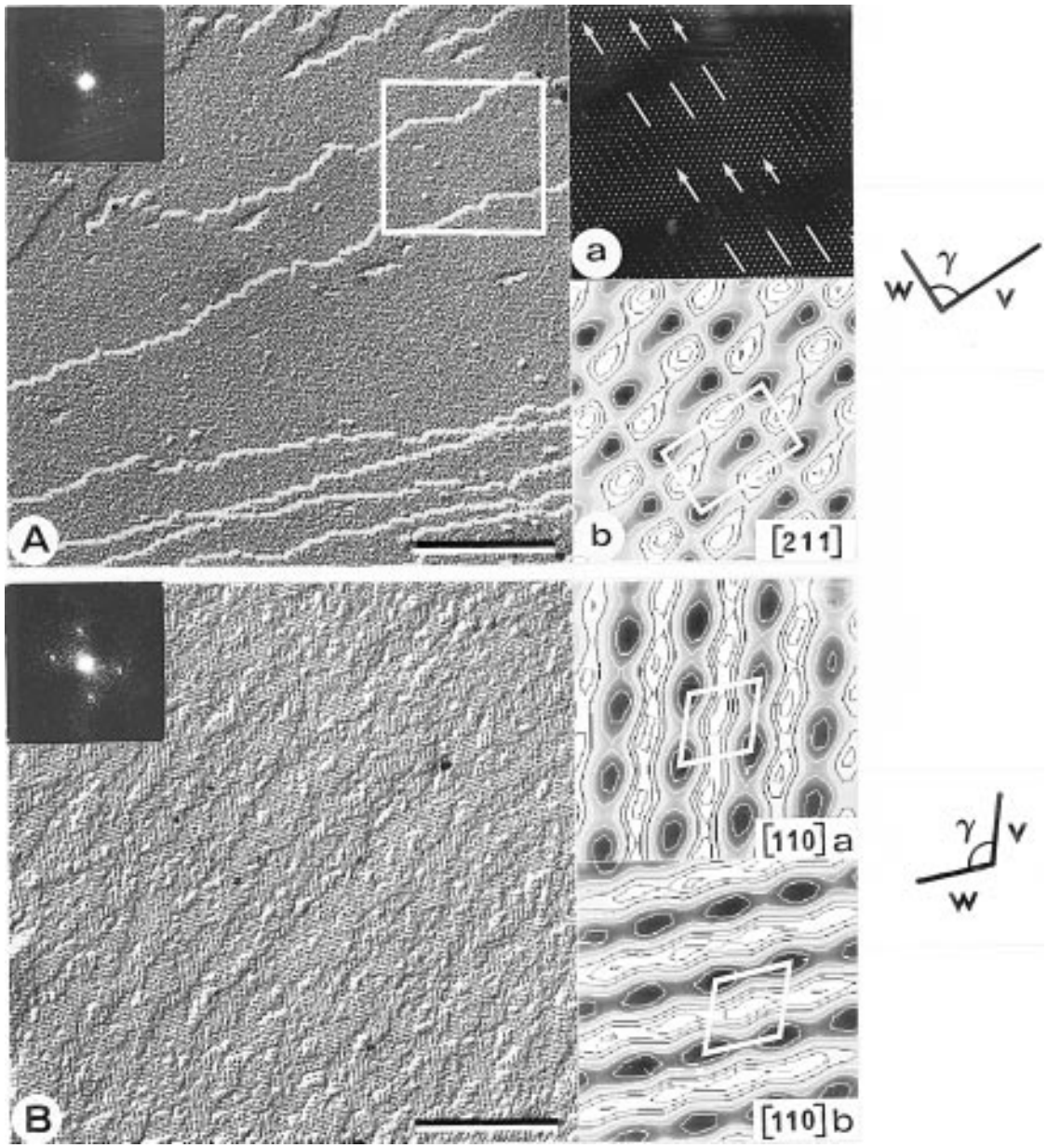

Figure 15. Freeze-fracture electron micrographs of [211] (A) and [110] (B) fracture domains for [AgSt(5−3,4)$_2$][DOS]. The optical diffraction of their central parts are shown in their upper left corners. Cross-correlation of the region delimited with a white square in (A), showing the shifts between successive [211] subdomains (arrows) is shown in the upper right corner (a) and the CCR-averaged motif in the lower right corner (b). The apparent 2-D lattice parameters for the [211] domains are $v = a\sqrt{2}$, $w = a\sqrt{3}/2$, $\gamma = 90°$, with $a = 6.85$ nm. The two CCR-averaged motifs corresponding to successive subdomains of the [110] domains ([110]a and [110]b) are shown at the right side of (B). The apparent 2-D lattice parameters are $v = w = a\sqrt{3}/2$, $\gamma = 109°28'$, with $a = 6.95$ nm. The bars in (A) and (B) represent 200 nm.

ence of different symmetry elements helping the determination of the space group of different cubic phases.

The techniques are applied here to the study of thermotropic cubic phases of the silver complexes under discussion, and some preliminary findings have recently been published.[41] Two such cubic phases and a hexagonal phase were studied for the complexes [Ag(St(*n*-3,4))$_2$][DOS] with $n = 5$ and $n = 6$ (cubic) and $n = 11$ (hexagonal). The freeze-fracture replicas of both cubic phases display almost identical patterns corresponding to different cleavage planes of three-dimensional crystals, and more or less extended relatively flat domains were commonly observed.

In many places, as expected, the replica displayed regularly ordered fracture surfaces which, accordingly to their optical diffraction patters and to the dimensions of their two-dimensional lattices, could be sorted in two classes of domains characteristic of the body-centered, $Ia\bar{3}d$ cubic phase (Q^{230}).[38a] One class corresponded to fracture domains that are perpendicular to the [211] crystallographic direction of this space group, the other to fracture domains perpendicular to the [110] crystallographic direction. The [211] domains are the most frequently observed and are usually fairly extended while the [110] domains are only sparingly observed and their surfaces looked like a mosaic of tiny subdomains.

The [211] fracture domains (Figure 15A) were almost flat and made of a succession of large successive cleavage planes, each of these subdomains displaying

(41) Donnio, B.; Bruce, D. W.; Delacroix, H.; Gulik-Krzywicki, T. *Liq. Cryst.* **1997**, *23*, 147.

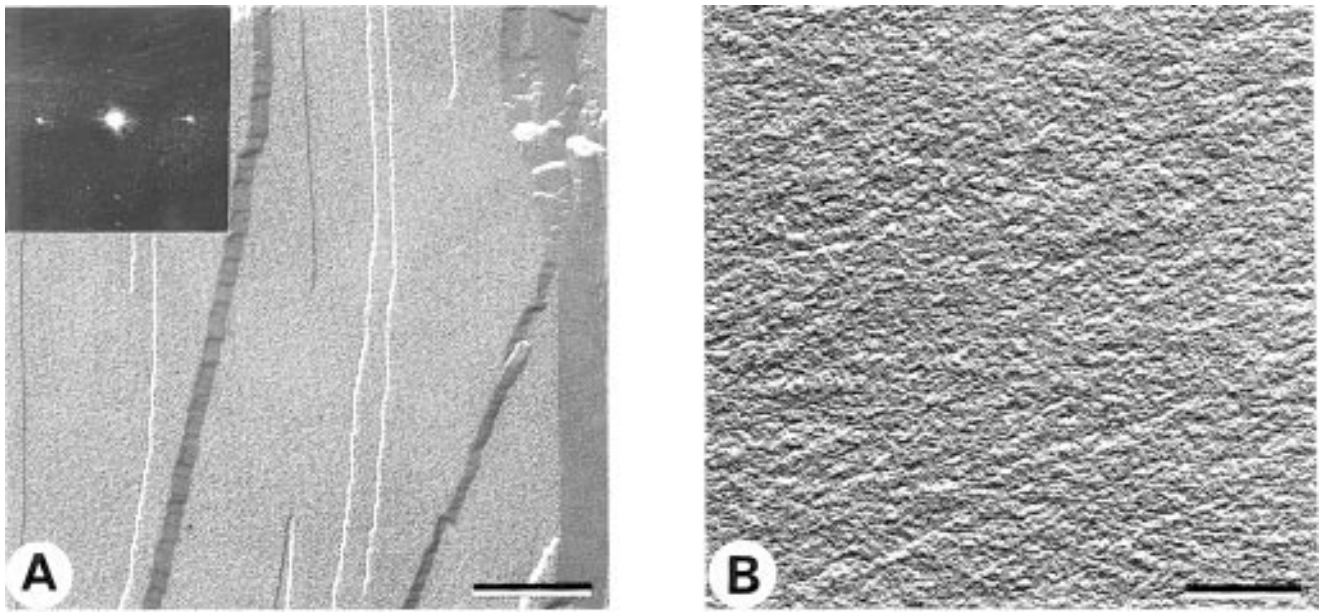

Figure 16. Figure-fracture electron micrographs of the columnar phase of [Ag{St(11−3,4)}$_2$][DOS] (A), with its optical diffraction shown in the upper left corner, and the isotropic phase of [Ag{St(6−3,4)}$_2$][DOS] (B). Notice the presence of regular striations for the columnar phase (A) and the amorphous appearance of isotropic phase (B). The bars represent 200 nm.

the same parallel striations. The correlation map (Figure 15A) showed that within a fracture domain, the successive subdomains had the same orientation and also contained the same rectangular 2-D periodic lattice of parameters ($v = a\sqrt{2}$, $w = a\sqrt{3}/2$, $\gamma = 90°$) that were consistent with the ideal values of this crystallographic plane. Furthermore, these correlation maps showed that the subdomains appeared as being (horizontally) shifted, one with respect to the others ($v/3 + w/2$). This apparent displacement could be easily related with the crystallographic relationship predicted between equivalent planes of the Q^{230} cubic structure taken perpendicularly to the [211] direction. As the [211] subdomains were of large size, correlation averaging could be performed efficiently and led to the average motif shown in Figure 15A.

The [110] fracture domains (Figure 15B) were rare and made of a complicated puzzle of small subdomains displaying lozenge-like striation. A thorough observation of these fracture domains revealed that the aspect of the subdomains were not unique and that two kinds of periodic motifs, having the same cell parameters ($v = w = a\sqrt{3}/2$, $\gamma = 109°29'$) could be observed. The low resolution of images of those distorted [110] fracture surfaces is revealed by the optical diffraction shown in the Figure 15B. As a consequence, the correlation averaging procedure was less easy to achieve in this case but eventually yielded to two distinct motifs [110]a and [110]b, characteristic for the [110] domains that are shown in the Figure 15B.

The unit-cell dimension computed from the micrographs, $a = 6.9 \pm 0.1$ nm, is fully compatible with the values obtained by X-ray diffraction ($a \approx 7.47$ nm) especially if one takes into account a frequently observed shrinking (5−10%) of the lattice due to freezing.[38]

Freeze-fracture electron micrographs of the columnar phase of [Ag(St(11−3,4))2][DOS] phase shown in Figure 16A, display characteristic for hexagonal type II (H_{II}) periodic striations, separation of which corresponds to the distance between hexagonally packed cylinders.[37]

The electron micrographs of an isotropic phase, such as that shown in Figure 16B, display only an amorphous appearance.

Conclusions

In this paper, we have therefore described in great detail the synthesis, mesomorphism, and characterization of a series of polycatenar complexes of silver(I). The mesomorphism is identified as predominantly cubic and hexagonal columnar by using optical microscopy, freeze-fracture electron microscopy, and X-ray diffraction. Studies by a combination of X-ray diffraction have shown that there are six complex molecules in the column repeat and that the faster-than-expected increase in the columnar cross section, *s*, may be explained by undulations in the columnar structure. The linear relationship between the volumes of the cubic and hexagonal phases and the proposed undulations allows a model to be presented for the transition between the two phases. The model successfully accounts for the observed epitaxial relationship between the two phases and is consistent with models proposed for related transitions in both lyotropic and thermotropic systems.

Freeze-fracture microscopy showed that it is possible to preserve the crystalline order of two- and three-dimensionally ordered high-temperature thermotropic phases during the entire freeze-fracture replication process and that when such preservation is achieved, image analysis of the micrographs (leading to the determination of the orientation of the different fracture planes, of their frequency and of the presence of symmetry elements) followed by the comparison with phases of known structure may be very useful for the structure determination of an unknown phase.

Experimental Section

All solvents and 4-methylpyridine were distilled prior to use according to the standard procedures.[42] Thus, dichloromethane was distilled from calcium hydride, tetrahydrofuran (THF) from sodium and benzophenone, toluene from sodium, metha-

nol from magnesium and iodine, and acetone from potassium permanganate. Diethyl ether was dried and stored over sodium wire. 4-Methylpyridine was distilled over sodium hydroxide and stored over sodium hydroxide pellets. Potassium carbonate was kept in the oven. All other chemicals were used as supplied.

Proton and carbon NMR spectra were recorded on a Brücker ACL250 spectrometer and referenced to external tetramethylsilane. Elemental analyses were performed by the University of Sheffield microanalytical service. IR were recorded on a Perkin-Elmer infrared spectrophotometer 684.

Analysis by DSC was carried out using a Perkin-Elmer DSC7 instrument using various heating rates. Mesomorphism was studied by hot-stage polarizing microscopy using a Zeiss Labpol microscope equipped with a Linkam TH600 hot-stage and PR600 temperature controller. All of the mesophases were characterized by their optical textures, and the hexagonal and body-centered cubic symmetries of the phases were confirmed by a combination of X-ray scattering studies and freeze-fracture electron microscopy.

The X-ray diffraction patterns were obtained with three different experimental setups; in all cases, the crude powder was filled in Lindemann capillaries of 1 mm diameter. For the characterization of the wide-angle region, a linear monochromatic Cu $K\alpha_1$ beam obtained with a sealed-tube generator (900 W) and a bent quartz monochromator was used. The diffraction patterns were registered with a curved counter "Inel CPS 120". Periodicities up to 60 Å could be measured, and the sample temperature was controlled within ±0.05 °C. The measurement of the periodicities were performed by using a linear monochromatic Cu $K\alpha_1$ beam obtained with a sealed-tube generator and a bent quartz monochromator. The diffraction patterns were registered on films; the cell parameter were calculated from the position of the reflection at the smallest Bragg-angle, which was in all cases the most intense. Periodicities up to 90 Å could be measured, and the sample temperature was controlled within ±0.3 °C. To check the existence of additional reflections at very small angles, patterns were registered for all samples, by using a linear Cu Kα-beam obtained with a rotating anode and passing through a Ni filter. In the geometry used, periodicities up to 200 Å could be measured. The diffraction patterns were registered on films and the sample temperature was controlled within ±0.3 °C. In each case, exposure times were between 1 and 48 h depending on the phase being observed and upon the specific reflections being sought (weaker reflections obviously taking longer to expose).

Dilatometric measurement were performed with a high-precision home-built apparatus with automatic computer-controlled operation, including data acquisition and temperature control within ±0.03 °C.[43] Relative variations of the specific volume could be detected with a resolution of 0.1%, and its absolute value determined with an accuracy of 0.01%

For freeze-fracture electron microscopy, a few milligrams of the powdered sample were placed on a thin copper holder maintained at a temperature corresponding to the presence of a phase to be studied and then rapidly quenched in liquid propane. The frozen sample was fractured at −125 °C, under a vacuum better than 10^{-6} Torr, using the liquid nitrogen cooled knife in a Balzers 301 freeze-etching unit. The replication was done using unidirectional shadowing, at an angle of 35°, with platinum−carbon, generating 1−1.5 nm mean metal deposit. The replicas were washed with organic solvents and distilled water and were observed using a Philips 301 electron microscope.

Image selection and processing has been already extensively described elsewhere[38] and needs just to be summarized here. Briefly, the micrographs are inspected in a search for ordered domains. The images of these domains were optically filtered, the dimensions of the 2-D lattices were determined, and their relative frequency was assessed. The crystallographic orientation of each domain is then determined. A few well-ordered domains were singled out, corresponding to the different previously observed orientations. Stereoviews are used to select the domains whose fracture plane is virtually parallel to the plane of the image. Further processing is used to improve to the signal-to-noise ratio. A few selected images are digitized, the subdomains are identified and the cell parameters computed from their Fourier transform. Each subdomain is then Fourier-filtered using those cell parameters. Finally an area is selected and analyzed using a cross-correlation averaging procedure.[44] The relationships between the different subdomains are analyzed by cross-correlating the domain with the averaged motif of one subdomain or by carefully Fourier-filtering the whole domain. It must be stressed that no symmetry operation is involved in the entire process.

General Procedures. Two different synthetic routes were used for the preparation of the ligands. Initially, we used a Heck coupling reaction between 3,4-dialkoxybromobenzene and 4-vinylpyridine (Figure 2). However, we later employed the condensation reaction (Figure 3) between 4-methylpyridine and 3,4-dialkoxybenzaldehyde, which we would now identify as the preferred route on account of improved yields, shorter reaction times, and easier purification.

Synthesis of 3,4-Dialkoxy-4′-stilbazole via the Heck Reaction. *Preparation of 3,4-Dihydroxybromobenzene (4-Bromocatechol).* A solution of boron tribromide in dichloromethane (1 mol dm^{-3}, 50 mmol) was added dropwise to a stirred, cooled (−78 °C) solution of 4-bromoveratrole (5 g, 23 mmol) in dichloromethane (60 cm^3). When the addition was complete, the mixture was allowed to warm to room temperature and was left stirring for one further hour. Distilled water (100 cm^3) was then added dropwise, and the dichloromethane fraction collected, washed with water (2 × 100 cm^3), and dried ($MgSO_4$). The solvent was removed under reduced pressure, and the resulting solid was triturated with pentane and crystallized from dichloromethane/pentane to give colorless crystals in quantitative yield.

Preparation of 3,4-Diheptoxybromobenzene. A solution of 1-bromoheptane (9.5 g, 53 mmol) in acetone (50 cm^3) was added dropwise to a stirred refluxing mixture of 4-bromocatechol (4.22 g, 22.3 mmol) and potassium carbonate (11 g, 80 mmol) in acetone (50 cm^3). After 36 h at reflux, the mixture was cooled and filtered through Celite, and the filtrate was reduced to dryness on a rotary evaporator; the resulting solid was dissolved in diethyl ether (100 cm^3). This solution was then washed with sodium hydroxide (70 cm^3, 10% w/w), distilled water (60 cm^3), and sodium chloride solution (50 cm^3, saturated) and then finally dried ($MgSO_4$). The solvent was removed, and the product was distilled (180 °C, 0.3 mmHg); the product slowly crystallized with time. The yield was 94% (8.1 g). Homologues with more than eight carbons in each chain were solid and were purified by crystallization from hot acetone.

All the other homologues were similarly prepared and obtained in similar yields. The ^1H, ^{13}C and IR data were as shown below. Microanalytical data were good and were made available to the referees.

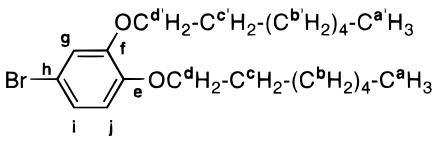

δ_H (250 MHz; $CDCl_3$) 0.92, 0.94 (a, a′, 2 t, ^3J = 6.3 Hz, 6 H), 1.45 (b, b′, m, 16 H), 1.81 (c, c′, m, 4 H), 3.90, 3.92 (d, d′, 2 t, ^3J = 6.3 Hz, 4 H), 6.69 (j, d, $^3J_{ji}$ = 8.1 Hz, 1 H), 6.94 (i, dd, $^3J_{ij}$

(42) Furniss, B. S.; Hannaford, A. J.; Smith, P. W. G.; Tatchell, A. R. *Vogel's Textbook of Practical Organic Chemistry*, 5th ed.; Longman Scientific and Technical; John Wiley and Sons Publishers: New York, 1989. Casey, M.; Leonard, J.; Lygo, B.; Procter, G. *Advanced Practical Organic Chemistry*; Blackie Academic and Professional: UK, 1990.

(43) Heinrich, B.; Halbwachs, A.; Skoulios, A.; Guillon, D., to be published.

(44) Saxton, W. O.; Frank, J. *Ultramicroscopy* **1977**, *2*, 219. Frank, J.; Goldfarb, W.; Eisenberg, D.; Baker, T. S. *Ultramicroscopy* **1978**, *3*, 283.

= 8.1 Hz, $^4J_{ig}$ = 2.0 Hz, 1 H), 6.96 (g, d, $^4J_{gi}$ = 2.0 Hz, 1 H). δ_C (62.9 MHz; $CDCl_3$) 14.1 (a, a′), 22.7, 26.0, 26.3, 29.2, 29.3, 29.4, 29.6, 31.8 (b, b′, c, c′), 69.4, 69.5 (d, d′), 112.8 (h), 115.2 (j), 117.0 (g), 123.4 (i), 148.4 (e), 150.1 (f).

Preparation of Di-3′,4′-heptoxy-4-stilbazole. A thick-walled Pyrex tube of the Fisher-Porter type and a Soxhlet apparatus (for purification) were used. The method is described in detail in ref 29. This procedure was used for all the members of this series. The products appeared as white or pale yellow solids in typically 40−50% yield.

3,4-Dialkoxy-4′-stilbazole, Method 2 (See Figure 3). *Preparation of the 3,4-Diheptoxybenzaldehyde.* A solution of 1-bromoheptane (10.7 g, 32 mmol) in butanone (20 cm^3) was added dropwise to a mixture of 3,4-dihydroxybenzaldehyde (2 g, 14.5 mmol) and potassium carbonate (12 g, 44 mmol) in butanone (50 cm^3), and the mixture was then refluxed (36 h). The resulting mixture was cooled and filtered through Celite, and the butanone evaporated under reduced pressure. The resulting solid was extracted into diethyl ether (100 cm^3) and the solution was washed with sodium hydroxide solution (70 cm^3, 10% w/w), distilled water (60 cm^3), and sodium chloride (50 cm^3 saturated) and finally dried ($MgSO_4$). The solvent was removed, and the product crystallized from hot acetone to give colorless crystals in 75% yield (3.6 g).

For the short-chain homologues (n = 2 and 3), an oil was obtained that was purified by column chromatography (silica gel, 90% dichloromethane/10% hexane) to give a colorless oil. The propoxy homologue slowly crystallized with time.

All the other homologues were similarly prepared and obtained in similar yields. The ^{1}H, ^{13}C, and IR data were as shown below. Microanalytical data were good and were made available to the referees.

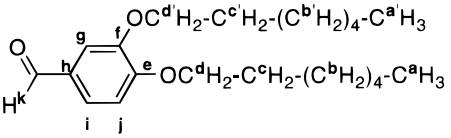

δ_H (250 MHz; $CDCl_3$) 0.89, 0.90 (a, a′, 2 t, ^3J = 6.7 Hz, 6 H), 1.39 (b, b′, m, 16 H), 1.82 (c, c′, m, 4 H), 4.04, 4.07 (d, d′, 2 t, ^3J = 6.7 Hz, 4 H), 6.94 (j, d, $^3J_{ji}$ = 7.9 Hz, 1 H), 7.38 (g, d, $^4J_{gi}$ = 2.1 Hz, 1 H), 7.41 (i, dd, $^3J_{ij}$ = 7.9 Hz, $^4J_{ig}$ = 2.1 Hz, 1 H), 9.81 (k, s, 1 H). δ_C(62.9 MHz; $CDCl_3$) 13.6, 13.9 (a, a′), 22.5, 25.9, 29.0, 29.2, 29.3, 31.4 (b, b′, c, c′), 69.1 (d, d′), 110.9 (g), 111.7 (j), 126.4 (i), 129.8 (h), 149.4 (f), 154.7 (e), 190.9 (k). IR (CsI/Nujol, cm^{-1}) $\nu_{C=O}$ 1690(s), $\nu_{C-H(aldehyde)}$ 2715 (w).

Preparation of Di-3′,4′-heptoxy-4-stilbazole. A mixture of diisopropylamine (16.7 mmol, 2.34 cm^3) and THF (5 cm^3) was added to the vessel cooled to −78 °C and stirred. Subsequently, a solution of butyllithium in hexane (1.6 mmol dm^{-3}, 10.6 cm^3) was added dropwise to the reaction mixture over a few minutes. After 30 min, a solution of 4-methylpyridine (13.6 mmol, 1.32 cm^3) in THF (10 cm^3) was added slowly. During the addition, a change of color to an intense orange could clearly be observed, indicating the lithiation of 4-picoline. The temperature was allowed to rise to −40 °C, and the mixture was left for 30 min. 3,4-Diheptoxybenzaldehyde (3.5 g, 10.5 mmol) dissolved in THF (10 cm^3) was then added dropwise to the lithiated picoline, during which the intense orange color slowly disappeared. The reaction mixture was allowed to rise to room temperature, and after stirring overnight, a solution of HCl (20 cm^3, 3% v/v) was added with vigorous stirring. The compound was extracted twice with diethyl ether or dichloromethane (2 × 50 cm^3), and the combined extracts were washed with water until the washing water was at pH 7. The solution was then dried ($MgSO_4$), and concentrated in vacuo to give the secondary alcohol intermediate as an oil. Prior to the dehydration step, the alcohol was refluxed in toluene (200 cm^3) for 1 h using a Dean−Stark in order to eliminate residual water. When cooled, pyridinium *p*-toluenesulfonate (3.42 g, 13.6 mmol) was added to the solution and the mixture refluxed overnight to give a brown oil after distillation of the solvent. The compound was extracted with dichloromethane (200 cm^3) and washed with water (5 × 150 cm^3) until a neutral pH was achieved. The product was purified by column chromatography (basic alumina, 90% dichloromethane/10% hexane). The yield was 68% (2.91 g) and the geometry of the double bond was exclusively trans (J_{AB} = 16.5 Hz).

Table 4. Microanalytical Data for 3′,4′-Dialkoxy-4-stilbazole

		(calcd) found		
n	yield	C	H	N
1	68	(74.7) 74.4	(6.3) 6.2	(5.8) 5.7
2	74	(75.8) 75.7	(7.1) 7.1	(5.2) 5.1
3	65	(76.7) 76.9	(7.8) 7.8	(4.7) 4.5
4	79	(77.5) 77.3	(8.4) 8.3	(4.3) 4.5
5	89	(78.1) 78.0	(8.8) 9.0	(4.0) 3.8
6	69	(78.7) 78.5	(9.2) 9.2	(3.7) 3.6
7	68	(79.2) 78.8	(9.6) 9.8	(3.4) 3.2
8	69	(79.6) 79.4	(9.9) 9.8	(3.2) 3.0
9	61	(79.9) 79.5	(10.2) 10.2	(3.0) 2.8
10	64	(80.3) 79.9	(10.4) 10.6	(2.8) 2.2
11	65	(80.6) 80.2	(10.6) 10.7	(2.7) 2.5
12	65	(80.8) 80.9	(10.8) 10.9	(2.5) 2.6

All the other homologues were similarly prepared and obtained in similar yields. All the analytical data are collected in Table 4 and the ^{1}H and ^{13}C were as follows. The protons of the pyridyl ring were analyzed as an AA′XX′ system.

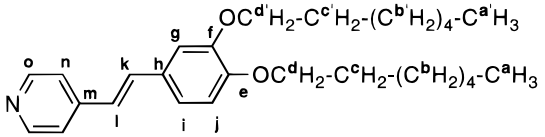

δ_H (250 MHz; $CDCl_3$) 0.90, 0.92 (a, a′, 2 t, ^3J = 6.3 Hz, 6 H), 1.38 (b, b′, m, 16 H), 1.85 (c, c′, m, 4 H), 4.01 (d, t, ^3J = 6.3 Hz, 2 H), 4.03 (d′, t, ^3J = 6.3 Hz, 2 H), 6.84 (l, AB, $^3J_{lk}$ = 16.5 Hz, 1 H), 6.86 (j, d, $^3J_{ji}$ = 8.0 Hz, 1 H), 7.03 (i, dd, $^3J_{ij}$ = 8.0 Hz, $^4J_{ig}$ = 2.0 Hz, 1 H), 7.07 (g, d, $^4J_{gi}$ = 2.0 Hz, 1 H), 7.22 (k, AB, $^3J_{kl}$ = 16.5 Hz, 1 H), 7.32 (n, AA′XX′, $|J_{no} + J_{no'}|$ = 6.1 Hz, 2 H), 8.53 (o, AA′XX′, $|J_{on} + J_{on'}|$ = 6.1 Hz, 2 H). δ_C (62.9 MHz; $CDCl_3$) 14.0 (a, a′), 22.6, 26.0, 29.1, 29.2, 29.3, 31.8 (b, b′, c, c′), 69.2 (d), 69.4 (d′), 111.8 (g), 113.4 (j), 120.6 (n), 120.9 (i), 123.7 (l), 129.1 (h), 133.2 (k), 145.0 (m), 149.3 (e), 150.0 (f), 150.2 (o).

In Table 3, the data correspond to the stilbazoles prepared according to the second procedure, although pure stilbazoles were obtained by either route.

Preparation of the Silver(I) Complexes. The synthesis of the silver complexes was achieved as shown in Figure 3.

A solution of di-3′,4′-heptoxy-4-stilbazole (500 mg, 1.22 mmol) in dichloromethane (10 cm^3) was added dropwise to a stirred suspension of AgDOS (250 mg, 0.67 mmol, from silver nitrate and sodium dodecyl sulfate in water) in dichloromethane (10 cm^3) and stirred (4 h, room temperature) with the vessel protected from the light. The mixture was then filtered through Celite, and the solvent removed under reduced pressure. The yellow viscous solid was crystallized from hot acetone and then recrystallized from methanol. The product was collected as a pale yellow solid in 75% yield (546 mg).

All the other homologues were similarly prepared and obtained in similar yields. All the analytical data are collected in Table 5 and the ^{1}H, ^{13}C and IR data were as follows.

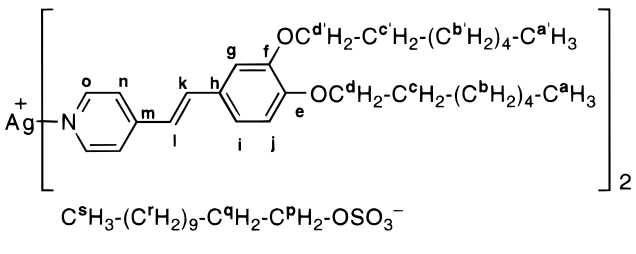

δ_H (250 MHz; $CDCl_3$) 0.84 (s, t, ^3J = 6.5 Hz, 3 H), 0.92 (a, a′, t, ^3J = 6.5 Hz, 12 H), 1.35 (b, b′, r, m, 50 H), 1.55 (q, m, 2

Table 5. Microanalytical Data for the Silver Complexes

		(calcd) found			
n	yield	C	H	N	S
1	72	(58.9) 58.8	(6.5) 6.5	(3.3) 3.2	(3.7) 3.9
2	83	(60.6) 60.2	(7.0) 6.9	(3.1) 3.0	(3.5) 3.3
3	79	(62.0) 61.9	(7.4) 7.5	(2.9) 2.9	(3.3) 3.1
4	78	(63.3) 63.0	(7.8) 7.5	(2.7) 2.8	(3.1) 3.0
5	79	(64.5) 64.0	(8.2) 8.0	(2.6) 2.6	(3.0) 3.1
6	78	(65.5) 65.3	(8.4) 8.1	(2.5) 2.5	(2.8) 3.0
7	75	(66.5) 66.0	(8.7) 8.4	(2.3) 2.4	(2.7) 2.7
8	83	(67.3) 67.1	(9.0) 8.8	(2.2) 2.3	(2.6) 2.6
9	86	(68.1) 68.2	(9.2) 9.4	(2.1) 2.2	(2.5) 2.3
10	74	(68.8) 68.9	(9.4) 9.2	(2.1) 2.1	(2.3) 2.3
11	83	(69.5) 68.9	(9.6) 9.8	(2.0) 2.0	(2.3) 2.3
12	83	(70.1) 69.7	(9.8) 9.6	(1.9) 1.8	(2.2) 2.3

H), 1.80 (c, c′, m, 8 H), 3.94, 3.97 (d, d′, t, ^3J = 6.5 Hz, 8 H), 4.15 (p, t, ^3J = 6.5 Hz, 2 H), 6.67 (l, AB, $^3J_{lk}$ = 16.7 Hz, 2 H), 6.71 (j, d, $^3J_{ji}$ = 8.0 Hz, 2 H), 6.88 (i, dd, $^4J_{ig}$ = 2.0 Hz, $^3J_{ij}$ = 8.0 Hz, 2 H), 6.95 (g, d, $^4J_{gi}$ = 2.0 Hz, 2 H), 7.15 (k, AB, $^3J_{kl}$ = 16.7 Hz, 2 H), 7.26 (n, AA′XX′, $|J_{no} + J_{no'}|$ = 6.5 Hz, 4 H), 8.66 (o, AA′XX′, $|J_{on} + J_{on'}|$ = 6.5 Hz, 4 H). δ_C (62.9 MHz; $CDCl_3$) 14.0 (a, a′), 14.1 (s), 22.7, 25.7, 26.1, 29.3, 29.4, 29.7, 31.2, 31.6 (b, b′, c, c′, r), 31.9 (q), 68.1 (p), 69.1, 69.4 (d, d′), 111.7 (g), 113.1 (j), 121.4 (n), 121.5 (i), 122.2 (l), 128.4 (h), 135.5 (k), 147.2 (m), 149.3 (e), 150.6 (f), 152.2 (o).

Acknowledgment. T.G.K. would like to thank J. C. Dedieu for his excellent technical assistance with electron microscopy, B.D. would like to thank the European Union for the award of a Human Capital and Mobility Category 20 Fellowship, and D.W.B. and D.G. acknowledge with pleasure support from both the British Council Alliance Scheme and the EU Human Capital and Mobility Network (Molecular Organization in Liquid Crystals Resulting from Particular Intermolecular Interactions, Ref No. ERB4050 PL 922749).

CM970300O